

Distinguishing general relativity and $f(R)$ gravity with the gravitational lensing Minkowski functionals

Chenxiaoji Ling,¹ Qiao Wang,¹ Ran Li,¹ Baojiu Li,² Jie Wang,¹ and Liang Gao^{1,2}

¹National Astronomical Observatories, Chinese Academy of Sciences, 20A Datun Road, Chaoyang, Beijing 100012, China

²Institute for computational Cosmology, Department of Physics,
Durham University, South Road, Durham DH1 3LE, UK

(Dated: August 25, 2021)

We explore the Minkowski functionals of weak lensing convergence map to distinguish between $f(R)$ gravity and the general relativity (GR). The mock weak lensing convergence maps are constructed with a set of high-resolution simulations assuming different gravity models. It is shown that the lensing MFs of $f(R)$ gravity can be considerably different from that of GR because of the environmentally dependent enhancement of structure formation. We also investigate the effect of lensing noise on our results, and find that it is likely to distinguish F5, F6 and GR gravity models with a galaxy survey of ~ 3000 degree² and with a background source number density of $n_g = 30$ arcmin⁻², comparable to an upcoming survey dark energy survey (DES). We also find that the $f(R)$ signal can be partially degenerate with the effect of changing cosmology, but combined use of other observations, such as the cosmic microwave background (CMB) data, can help break this degeneracy.

PACS numbers: 04.50.Kd,95.30.Sf,95.36.+x,98.65.Dx

I. INTRODUCTION

It is fundamentally important to explain the observed accelerating expansion of the Universe [1, 2]. In the current understanding, this accelerating expansion either is driven by an exotic dark energy in the framework of general relativity (hereafter GR) or indicates that GR needs to be modified on large scales [3]. A well-studied example of the latter scenario is the so-called $f(R)$ gravity [4], in which the Ricci scalar R in the standard Einstein-Hilbert action is replaced by a function $f(R)$. In most $f(R)$ models studied so far, the difference between $f(R)$ and R remains roughly a constant throughout the cosmic history, therefore accelerating the expansion of the Universe like in the standard Λ CDM paradigm.

Although the background expansion history in $f(R)$ models could be practically indistinguishable from that of Λ CDM, the structure formation can be very different for these two scenarios. In $f(R)$ gravity, df/dR is nontrivial and behaves like a dynamical scalar field, which propagates a "fifth force" between matter particles. The strength of this fifth force can be maximally 1/3 of that of Newtonian gravity, but it is usually weaker because of the well-known chameleon mechanism [5], which strongly suppresses it in regions with high matter density (or deep gravitational potential). The idea is that any deviation from standard GR gravitational law would be "screened" and therefore undetectable in the solar system, in which the validity of GR has been confirmed experimentally to very high precision. However, it is worth stressing that the behavior of the fifth force in solar-like systems relies heavily on what is going on at much larger scales such as the Milky Way galaxy, its dark matter halo and beyond. Although recent works have demonstrated the encouraging potential of constraining $f(R)$ gravity using such systems [6, 7], better understandings of the large-scale behavior of the scalar field will be needed before quantitative conclusions are finally drawn. In this sense, it is crucial to study the cosmological behavior of $f(R)$ gravity, as a means to constrain gravity using the constantly improving

cosmological data (see [8] for a recent review).

Previous works on this subject using statistics of large scale structure often compare matter power spectrum and correlation functions of matter distribution in GR and $f(R)$ gravity [see, e.g., 9–12]. In this work, we investigate the topological difference in the lensing convergence κ map between GR and $f(R)$ universes. The lensing κ map reflects the projected mass distribution of the Universe; its topological information can be described using Minkowski functionals (MFs) [13, 14]. In recent works, MFs have been extensively used to study the geometry properties of cosmic field ([15–20]). It has been shown that lensing MFs contain significant information beyond other statistical quantities, e.g. the power spectrum [21], thus might provide a promising way to distinguish $f(R)$ and GR model.

In this paper, we construct mock lensing maps with a set of $f(R)$ and GR cosmological simulations using the ECOSMOG [22] code, and investigate whether or not the MFs of lensing map can be used to distinguish different gravity models. In addition, we investigate the degeneracy effect between cosmic parameters and cosmic models.

This paper is organized as follows. In Section II, we briefly introduce the general $f(R)$ models and the N -body simulations used in this work. In Section III, we present our algorithm to calculate the MFs. In Section IV we present our results. In Section V we discuss the effect of cosmic parameters, and we give a summary in Section VI.

II. THE $f(R)$ COSMOLOGY

A. The $f(R)$ gravity model

The $f(R)$ gravity model is a simple generalization of standard Λ CDM paradigm by replacing the Ricci scalar R in the Einstein-Hilbert action with an algebraic function of R . The

modified action can be written as:

$$S = \int d^4x \sqrt{-g} \left\{ \frac{M_{PI}^2}{2} [R + f(R)] + \mathcal{L}_m \right\}, \quad (1)$$

in which M_{PI} is the reduced Planck mass, $M_{PI}^{-2} = 8\pi G$, G is Newton's constant, g is the determinant of the metric $g_{\mu\nu}$ and \mathcal{L}_m is the Lagrangian density for matter fields.

There is plenty of literature about the derivation and properties of the modified Einstein equations in $f(R)$ gravity, and here we shall not repeat the details. Instead, we simply present the equations that are directly relevant to the cosmic structure formation. These are the modified Poisson equation:

$$\nabla^2 \Phi = \frac{16\pi G}{3} a^2 \delta\rho_m + \frac{a^2}{6} \delta R(f_R), \quad (2)$$

and the equation of motion (EoM) of the scalar field $f_R \equiv df(R)/dR$:

$$\nabla^2 f_R = -\frac{a^2}{3} [\delta R(f_R) + 8\pi G \delta\rho_m], \quad (3)$$

in which

$$\delta R \equiv R - \bar{R}, \quad \delta\rho_m \equiv \rho_m - \bar{\rho}_m. \quad (4)$$

Φ denotes the gravitational potential, ρ_m is the total density of matter (cold dark matter and baryons), and an overbar denotes the background average. a is the cosmic scale factor and $a = 1$ at present.

The $f(R)$ model has a GR limit, which is given by $f_R \rightarrow 0$. In this limit, the scalar field f_R becomes nondynamical (identically zero); Eq. (3) gives the GR relation $\delta R = -8\pi G \delta\rho_m$ and Eq. (2) reduces to the standard Poisson equation:

$$\nabla^2 \Phi = 4\pi G a^2 \delta\rho_m. \quad (5)$$

For general $f(R)$ gravity, on the other hand, the scalar field f_R has a complicated behavior, and leads to an environmentally dependant effective Newton's constant G_{eff} .

As described in the introduction, local tests of gravity based on solar system observations put a tight constraint on any deviation from the Newtonian gravity. The chameleon mechanism is introduced to evade the constraint by varying G_{eff} in different environments. In dense regions, δf_R becomes negligible, and one has

$\delta R(f_R) \approx -8\pi G \delta\rho$, thus Eq. (2) returns to the GR equation, Eq. (5). In underdense environments, the $\delta R(f_R)$ term in Eq. (2) becomes small and the Eq. (2) turns into:

$$\nabla^2 \Phi = \frac{16}{3} \pi G a^2 \delta\rho, \quad (6)$$

where the effective Newton's constant is enhanced by a factor of $1/3$ ($G_{\text{eff}} = 4G/3$) compared to its value in dense environments.

Note that the maximum enhancement of G in $f(R)$ gravity is always $1/3$, independent of the functional form of $f(R)$.

$f(R)$, on the other hand, determines how G_{eff} changes from G to $4G/3$ when environmental density changes. Therefore, the form of $f(R)$ is crucial for a given model. To date, various $f(R)$ functions have been designed to explain the accelerated cosmic expansion while evading solar system constraints, of which the most wellstudied is the one proposed by [23]:

$$f(R) = -M^2 \frac{c_1 (-R/gM^2)^n}{c_2 (-R/M^2)^n + 1}, \quad (7)$$

where $M^2 \equiv H_0^2 \Omega_m$ with H_0 the Hubble constant, Ω_m is the matter density parameter, and n is an integer parameter which is normally set to 1, though other values have been studied as well. To match¹ the expansion of a standard Λ CDM universe, the dimensionless parameters c_1 and c_2 should satisfy:

$$\frac{c_1}{c_2} = 6 \frac{\Omega_\Lambda}{\Omega_m}, \quad (8)$$

where Ω_Λ is the current dark energy density parameter.

In any reasonable cosmological model, we have $-\bar{R} \gg M^2$, and so \bar{f}_R can be simplified as:

$$f_R \simeq -\frac{nc_1}{c_2} \left(\frac{M^2}{-R} \right)^{n+1}. \quad (9)$$

Therefore, the model can be described by two free parameters, n and c_1/c_2 , and the latter is determined by f_{R0} , the value of f_R today.

B. Numerical simulations

Numerical simulations used in this study include three high resolution cosmological N -body simulations, two of which assume $f(R)$ gravity and one assumes Λ CDM. For two different $f(R)$ simulations, we have fixed the model parameter n to be 1 but varied the parameter f_{R0} by $|f_{R0}| = 1.289 \times 10^{-5}$ and 1.289×10^{-6} , which will hereafter be referred to as F5 and F6 model, respectively. All simulations evolve 1024^3 particles in a $250 h^{-1} \text{Mpc}$ cubic volume and start from exactly the same initial conditions at $z = 49.0$. The simulations were performed with the adaptive mesh refinement code ECOSMOG [22]. The cosmological parameters assumed to generate initial conditions are $\Omega_m = 0.267$, $\Omega_\Lambda = 0.733$, $h = 0.71$, $n_s = 0.958$ and $\sigma_8 = 0.801$, in which $h = H_0/(100 \text{km/s/Mpc})$, n_s is the spectral index of the primordial power spectrum and σ_8 is the rms density fluctuation within spherical tophat windows of radius $8 h^{-1} \text{Mpc}$. In this work, we place source galaxy at $z = 1$ and use the snapshot at $z \approx 0.1$ to construct lensing κ maps.

¹ We note that this is an approximate match, with an error of order f_R , which is practically too small to be observable. As mentioned earlier, it is possible to have an exact Λ CDM expansion history in $f(R)$ gravity, but the corresponding form of $f(R)$ is more complicated.

III. THE MINKOWSKI FUNCTIONALS (MFS) OF WEAK LENSING κ MAP

A. Weak lensing convergence map

Weak lensing observations measure small distortions on the shapes of background galaxies, which can be used to generate convergence κ map. The convergence map $\kappa(\mathbf{x})$ is related to projected density map $\Sigma(\mathbf{x})$ as:

$$\kappa(\mathbf{x}) = \frac{\Sigma(\mathbf{x})}{\Sigma_{cr}}, \quad (10)$$

with the critical surface density

$$\Sigma_{cr} = \frac{c^2}{4\pi G} \frac{D_s}{D_l D_{ls}}, \quad (11)$$

in which D_{ls} is the angular diameter distance between source galaxies and the lens, and D_l and D_s are the angular diameter distances from the observer to the lens and to the sources. c is the speed of light.

To generate a theoretical convergence map, we project particles in the whole simulation box onto a plane. Next we employ the cloud in cell (CIC) method to project dark matter particles to a 5000^2 grid surface density map. On average, there are about 43 particles on each grid, the grid separation is about $50h^{-1}kpc$. Then we convert the surface density map to convergence map by assuming our lens plane to be at $z = 0.1$, and all source galaxies at redshift $z = 1$. The total sky area of our mock lensing observation is about 3000 degree², comparable to forthcoming dark energy surveys (e.g., LSST [24] and Euclid [25]).

In real observations, the intrinsic ellipticity of source galaxies introduces noise to the convergence map. The Gaussian smoothing is often adopted to suppress the small scale noise. The uncertainties of a smoothed κ map are specified by the number density of source galaxies, n_g , and the smoothing aperture size θ_G . van Waerbeke 2000 [26] shows that the noise can be approximated by a Gaussian distribution with rms:

$$\sigma_{noise}^2 = \frac{\sigma_\epsilon^2}{4\pi\theta_G^2 n_g}, \quad (12)$$

where σ_ϵ^2 is the rms amplitude of the source intrinsic ellipticity distribution.

To simulate a more realistic convergence map, we first smooth our convergence map with the Gaussian window. We then add the noise resulting from intrinsic ellipticity of source galaxies using Eq.(12). Following [27], we set $\sigma_\epsilon = 0.4$.

To investigate the effect of smoothing scale on our results, we adopt three different smoothing scale $\theta_G = 0.5, 1$ and 5 arcmin. For n_g , we adopt two values: $n_{g1} = 30 \text{ arcmin}^{-2}$ for upcoming surveys such as DES and $n_{g2} = 100 \text{ arcmin}^{-2}$ for future more ambitious surveys.

B. Minkowski functionals

Minkowski functionals provide morphological statistics for any given smoothed random field characterized by a certain

threshold ν . Compared with traditional power spectrum methods, MFs contain not only information of spatial correlation of a random field, but also information of topology and object shapes. For a \mathbb{R}^n field one can get $n + 1$ MFs V_i . Weak lensing convergence map is a two-dimensional field, thus 3 MFs can be defined, namely V_0, V_1 , and V_2 .

For a smoothed field $u(\mathbf{x})$ in a 2D space, we define the area Q_ν and boundary ∂Q_ν to be:

$$Q_\nu \equiv \{\mathbf{x} \in \mathbb{R}^2 | u(\mathbf{x}) > \nu\}, \quad \partial Q_\nu \equiv \{\mathbf{x} \in \mathbb{R}^2 | u(\mathbf{x}) = \nu\}.$$

Then, MFs can be written as follows:

$$V_0(\nu) = \int_{Q_\nu} d\Omega, \quad (13)$$

$$V_1(\nu) = \int_{\partial Q_\nu} \frac{1}{4} dl, \quad (14)$$

$$V_2(\nu) = \int_{\partial Q_\nu} \frac{1}{2\pi} \kappa_c dl. \quad (15)$$

V_0 is the area of Q_ν , V_1 is the total boundary length of Q_ν and V_2 is the integrated geodesic curvature κ_c along the boundary.

We follow the method described in [21, 28] to calculate the MFs from the pixelated maps. On each grid, we calculate:

$$\mathcal{I}_0(\nu, p_j) = \Theta(u - \nu), \quad (16)$$

$$\mathcal{I}_1(\nu, p_j) = \frac{1}{4} \delta(u - \nu) \sqrt{u_{,x}^2 + u_{,y}^2}, \quad (17)$$

$$\mathcal{I}_2(\nu, p_j) = \frac{1}{2\pi} \delta(u - \nu) \frac{2u_{,x}u_{,y}u_{,xy} - u_{,x}^2u_{,yy} - u_{,y}^2u_{,xx}}{u_{,x}^2 + u_{,y}^2}, \quad (18)$$

where u_x, u_y are the two partial derivatives of $u(\mathbf{x})$. The numerical MFs of V_i can be computed by summing integrands over all pixels:

$$V_i(\nu) = \frac{1}{N_{pix}} \sum_{j=1}^{N_{pix}} \mathcal{I}_i(\nu, p_j), \quad (19)$$

In the above, Θ is the Heaviside step function. For the bin width Δ_ν , the delta function can be numerically calculated as follows:

$$\delta_N(\nu) = (\Delta_\nu)^{-1} [\Theta(\nu + \Delta_\nu/2) - \Theta(\nu - \Delta_\nu/2)]. \quad (20)$$

Note that the numerical MFs, Eq.(19), is actually the surface density of Eqs.(13), (14) and (15). In what follows, we refer to both of them as MFs and notation V_i .

IV. RESULTS

In Fig. 1, we show the MFs of surface density from our simulations. The MFs are plotted as functions of surface density in unit of mean surface density, Σ_{mean} . The overall shapes of MF curves of the $f(R)$ and GR models are similar. However, the amplitude of MFs of the $f(R)$ surface density map is higher at $\Sigma/\Sigma_{\text{mean}} > 2$. For the F6 case, V_0 is $\sim 10\%$ higher than that of GR model at $\Sigma/\Sigma_{\text{mean}} \sim 3 - 5$, while in denser regions ($\Sigma/\Sigma_{\text{mean}} > 15$) the V_0 of both models are almost identical. On the other hand, the difference in V_0 between F5 and GR increases with $\Sigma/\Sigma_{\text{mean}}$ and persists to larger density. At $\Sigma/\Sigma_{\text{mean}} \sim 20$, the V_0 of F5 model is about 60% larger than that of GR model. The V_1 and V_2 of F5 and F6 models show similar trends.

The apparent differences shown here reflect the environmentally dependent structure formation in universes with different gravity theories. As is shown in Reference [29], compared with the GR universe, there are more massive halos and larger size voids in $f(R)$ models because of the enhanced gravity in low density environments. As a result, the surrounding regions (including the filaments) of dark matter halos are denser in $f(R)$ gravity than in GR. Therefore, in $f(R)$ models, V_0 , which represents the area of regions with density higher than certain threshold, is smaller than that of GR in the low density regions ($\Sigma/\Sigma_{\text{mean}} < 1$), but is larger at relatively high density regions. For F6, in very high density regions, the chameleon screening ensures that both the gravity and MFs are similar to the results in GR.

The difference in V_1 and V_2 can also be explained in the similar way. However, unlike V_0 , V_1 and V_2 encode additional information on topology (which describes connectivity) of the κ map. As an example, the turn over trend in the lower panel of V_1 indicates transition of the topology of κ map from the isolated halo dominated case to the voids dominated one.

In real observations, noise resulting from the intrinsic ellipticity distribution of galaxies contaminates the lensing κ map. Gaussian smoothing is usually adopted to suppress the noise; however, it will also mix the MFs of different density thresholds.

In Fig. 2, we show the MFs of the simulated κ maps without taking into account the noise. We apply smoothing to the map with different smoothing scales, $\theta_G = 0.5, 1$ and 5 , respectively. Ref. [27] claimed that for cluster survey, the best smoothing scales is $\sim 1 \text{ arcmin}$. We find that the amplitudes of MFs at high density regions decrease significantly while the Poisson noises increase dramatically at the same region. This is because the smoothing procedure reduces total area of high density region. We conclude that a small smoothing scale is better for measuring MFs.

We show MFs of the κ map in Fig. 3 by taking into account the noise. Here we adopt two different noise cases, $n_g = 30$ and $n_g = 100$, in order to investigate effects of different noise levels on our results. For comparison we also include the case without noise. In the figure, we use a smoothing scale of $1'$ and generate 100 maps using different background noises which sharing the same standard deviation σ_{noise} . The shaded regions show the standard deviation of MFs, which is an esti-

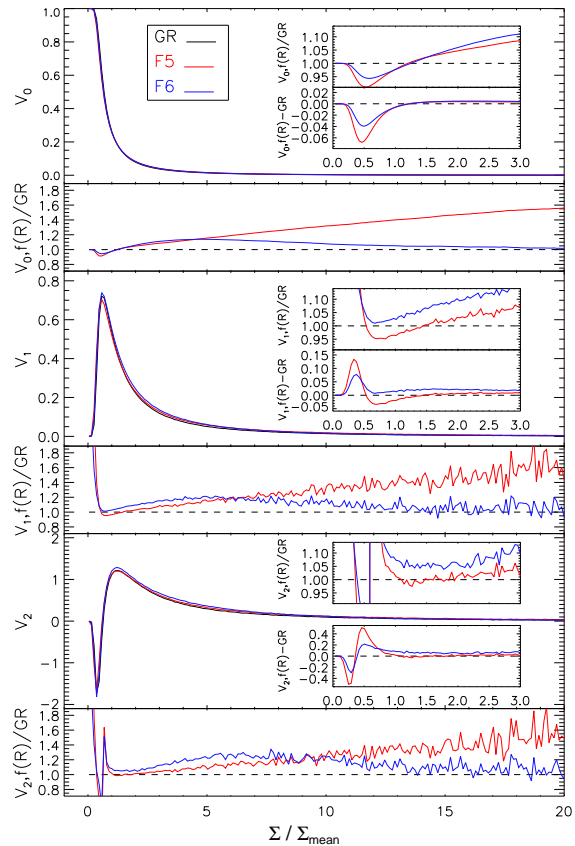


FIG. 1: The MFs of surface density maps as a function of surface density normalized to mean of the universe Σ_{mean} for our $f(R)$ and GR simulations. The black solid, red dashed, and blue dotted lines represent result for GR, F5 and F6 simulation, respectively. Interior small figures each panel show the ratios between GR and $f(R)$ simulations and the residuals as a function of surface density.

mation of the noise level. We note that the noise map due to intrinsic galaxy shapes can be approximated with a Gaussian map, which migrate into MFs, thus suppressing the difference between $f(R)$ and GR models. However, this effect is less important in dense regions ($\kappa > 0.015$). Therefore, it is still possible to distinguish the F5, F6 and GR models in high density regime. It is also interesting to see that even for the higher noise level, where $n_g = 30 \text{ arcmin}^{-2}$, the difference among different gravity models is still much larger than the observational lensing noise, indicating that weak lensing MFs can be a powerful tool to distinguish the $f(R)$ and GR models with upcoming galaxy surveys.

We further tested the evolution of lensing MFs with redshift. For this we fixed the source galaxy at $z = 1$ and employed four snapshots at different lens redshifts ($z = 0.8, 0.5, 0.2$ and 0.1 respectively). Figure 4 presents the results, where for simplicity we have used the same source galaxy density ($n_g = 30$) and smoothing scale ($1'$). The amplitudes of V_1 and V_2 of both GR and $f(R)$ gravity increase with time, and the relative differences of MFs between F5 and GR grow from 15% (at $z = 0.8$) to $50 \sim 60\%$ (at $z = 0.1$). The same trend is

found for F6 but the deviation from GR is much weaker. The results suggest that even with a more realistic line-of-sight integration to fully account for the matter distribution, we expect the model difference to be still present. Note that such an integration would somewhat distort the results and suppress the non-Gaussianity of the signal.

V. THE EFFECT OF COSMIC PARAMETERS

In this work, we have mainly focused on the difference between the MFs for $f(R)$ gravity and GR, but note that this signal could in principle be degenerate with the effect of changing cosmology [30]. To gain a rough idea of this degeneracy, we have employed two additional simulations: the Millennium simulation (MS) and a MS-W7 simulation. These simulations are identical on the simulation box and mass resolution, but with the cosmology changed from WMAP1 [31] to WMAP7 [32]. Because these two simulations are carried out by different simulation codes from $f(R)$ and GR runs, this code changing could bring about another effect in the MFs' measurement. We think it is better to check the effect of changing cosmology and changing gravity models individually, we present the comparison between two MS runs and comparison between different gravity models separately.

In Fig. 5, we compare the ratios of MFs for F5/GR (dotted lines), F6/GR (dashed lines) and WMAP1/WMAP7 (solid lines). The results of the noise-free case are shown in the left panels, while the right panels are the results assuming a source galaxy number density of 30. We find that the change of cosmology from WMAP7 to WMAP1 can have a similar impact as having F5 instead of GR as the gravity model. However, with the precision of current observations, the WMAP1 and WMAP7 cosmologies can be distinguished by using CMB data alone. In the cases of F6 and F5, the CMB power spectra are practically the same as GR predictions with the same cosmological parameters. Therefore, the CMB constraints on those cosmological parameters can be used to break the degeneracy above.

VI. SUMMARY

In this work, we make use of high-resolution $f(R)$ (F5, F6) and GR simulations to generate mock lensing κ map by taking

into account different noise levels. We find that due to environmental dependent nature of $f(R)$ gravity, the MFs of their κ maps show considerable deviation from the GR case. We also investigate the effect of lensing noise on our results, and find that while noise due to limited background source density induce pollution to the κ map, the difference between F5, F6 and GR gravity models can still be distinguished with a survey of ~ 3000 degree² area and with a background source number density $n_g = 30$ arcmin⁻². Such a requirement can be achieved by upcoming lensing surveys. We compared the effect of changing cosmological parameters and found that it can partly degenerate with the signal found in modified gravity. However, combined use of CMB data can help to break this degeneracy. Our results hence suggest that the MFs of lensing κ map will be a powerful tool to study the nature of gravity in the future.

Acknowledgements

We acknowledge support from the National Natural Science Foundation of China (NSFC) Grant No. 11303033, No.11103011, No.11373029, No.11390372, No.11403035, No. 11261140641, the Strategic Priority Research Program "The Emergence of Cosmological Structure" of the Chinese Academy of Sciences (CAS) (No. XDB09000000), MPG partner Group family. R.L. acknowledges the support from Youth Innovation Promotion Association of CAS. J.W. acknowledges supports from the Newton Alumni Fellowship, the 1000-young talents program, the 973 program grant No. 2013CB837900, No.2015CB857005, the CAS grant(No. KJZD-EW-T01). L.G. acknowledge a Science and Technology Facilities Council (STFC) Advanced Fellowship, as well as the hospitality of the Institute for Computational Cosmology (ICC) at Durham University. We thank the anonymous referee for comments which helped us to improve the paper. The simulations in this work used the DiRAC Data Centric system at Durham University, operated by the ICC on behalf of the STFC DiRAC HPC Facility (www.dirac.ac.uk). This equipment was funded by BIS National E-infrastructure Capital Grant NO.ST/K00042X/1, STFC Capital Grant NO.ST/H008519/1, and STFC DiRAC Operations Grant NO.ST/K003267/1 and Durham University. DiRAC is part of the National E-Infrastructure.

-
- [1] A. G. Riess, A. V. Filippenko, P. Challis, A. Clocchiatti, A. Diercks, P. M. Garnavich, R. L. Gilliland, C. J. Hogan, S. Jha, and R. P. Kirshner. *Astron. J.*, 116:1009, (1998).
 - [2] P. M. Garnavich, S. Jha, P. Challis, A. Clocchiatti, A. Diercks, A. V. Filippenko, R. L. Gilliland, C. J. Hogan, R. P. Kirshner, and B. Leibundgut. *Astronophys. J.*, 509:74, (1998).
 - [3] T. Clifton, P. G. Ferreira, A. Padilla, and C. Skordis. *Physics Reports*, 513:1, (2012).
 - [4] S. M. Carroll, A. De Felice, V. Duvvuri, D. A. Easson, M. Trodden, and M. S. Turner. *Phys. Rev. D*, 71:063513, (2005).
 - [5] J. Khoury and A. Weltman. *Phys. Rev. D*, 69:044026, (2004).
 - [6] A. C. Davis, E. A. Lim, J. Sakstein, and D. J. Shaw. *Physics Review D*, 85:123006, (2012).
 - [7] J. Bhuvnesh, V. Vinu, and J. Sakstein. *Astronophys. J.*, 779:39, (2013).
 - [8] L. Lombriser. *Ann. Phys. (Berlin)*, 526:259, (2014).
 - [9] H. Oyaizu, M. Lima, and W. Hu. *Phys. Rev. D*, 78:123524, (2008).
 - [10] G.-B. Zhao, B. Li, and K. Koyama. *Phys. Rev. D*, 83:044007, (2011).

- [11] B. Li, W. A. Hellwing, K. Koyama, G.-B. Zhao, E. Jennings, and C. M. Baugh. *Mon. Not. R. Astron. Soc.*, 428:743, (2013).
- [12] W. A. Hellwing, B. Li, C. S. Frenk, and S. Cole. *Mon. Not. R. Astron. Soc.*, 435:2806, (2013).
- [13] K. R. Mecke, T. Buchert, and H. Wagner. *Astron. Astrophys.*, 288:697, (1994).
- [14] J. Schmalzing, M. Kerscher, and Buchert. arxiv:astro-ph/9508154v2.
- [15] J. Schmalzing and K. M. Gorski. *Mon. Not. R. Astron. Soc.*, 297:355, (1998).
- [16] J. Schmalzing, S. Gottlber, A. A. Klypin, and A. V. Kravtsov. *Mon. Not. R. Astron. Soc.*, 309:1007, (1999).
- [17] C. Hikage, J. Schmalzing, T. Buchert, Y. Suto, I. Kayo, A. Taruya, M. S. Vogeley, F. Hoyle, III Gott, J. R., and J. Brinkmann. *Publications of the Astronomical Society of Japan*, 55:911, (2003).
- [18] S. Codis, C. Pichon, D. Pogosyan, F. Bernardeau, and T. Matsumoto. *Mon. Not. R. Astron. Soc.*, 435:531, (2013).
- [19] M. Kerscher, J. Schmalzing, T. Buchert, and H. Wagner. *Astron. Astrophys.*, 333:1, (1998).
- [20] A. Petri, Z. Haiman, L. Hui, M. May, and J. M. Kratochvil. *Phys. Rev. D*, 88:123002, (2013).
- [21] J. M. Kratochvil, E. A. Lim, S. Wang, Z. Haiman, M. May, and K. Huffenberger. *Astron. Astrophys.*, 85:103513, (2012).
- [22] B. Li, G.-B. Zhao, R. Teyssier, and K. Koyama. *J. Cosmology. Astropart. Phys.*, 01:051, (2012).
- [23] W. Hu and I. Sawicki. *Phys. Rev. D*, 76:064004, (2007).
- [24] P. A. Abell *et al.* (lsst science and lsst project collaborations), arxiv:0912.0201.
- [25] A. Refregier *et al.* arxiv:1001.0061.
- [26] L. van Waerbeke. *Mon. Not. R. Astron. Soc.*, 313:524, (2000).
- [27] T. Hamana, M. Takada, and N. Yoshida. *Mon. Not. R. Astron. Soc.*, 350:893, (2004).
- [28] E. A. Lim and D. Simon. *J. Cosmol. and Astropart. Phys.*, 01:048, (2012).
- [29] B. Li, G. B. Zhao, and K. Koyama. *Mon. Not. R. Astron. Soc.*, 421:3481, (2012).
- [30] M. Shirasaki and N. Yoshida. *Astronophys. J.*, 786:43, (2014).
- [31] V. Springel, S. D. M. White, and A. Jenkins. *Nature(London)*, 435:629, (2005).
- [32] Q. Guo, S. White, R. E. Angulo, and B. Henriques. *Mon. Not. R. Astron. Soc.*, 428:1351, (2013).

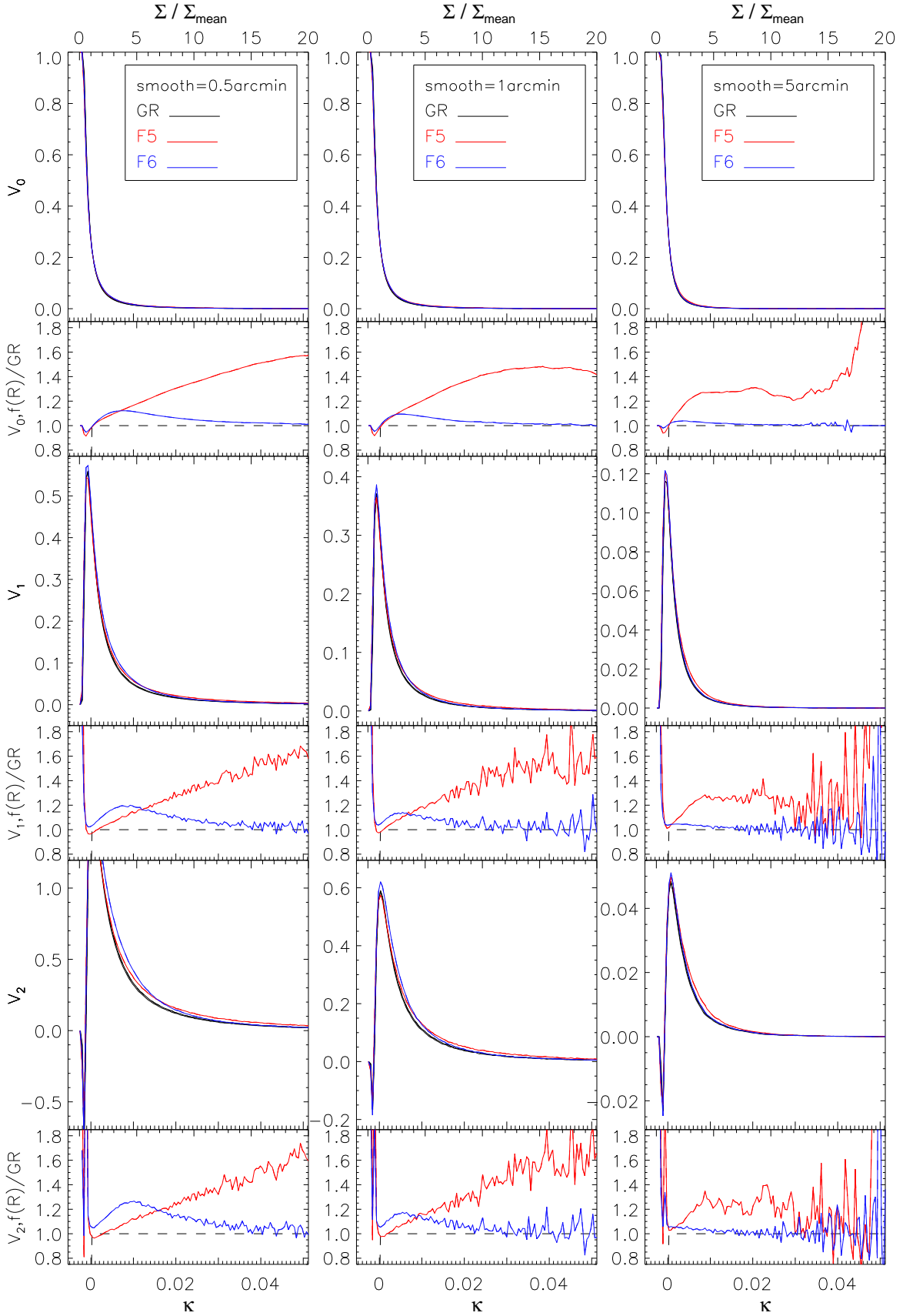


FIG. 2: The MFs of the noiseless κ maps as a function of κ (lower axis) and Σ/Σ_{mean} (upper axis). The black solid, red dashed, and blue dotted lines represent result of GR, F5 and F6 models respectively. The panels from left to right show results with different smoothing scales: 0.5', 1' and 5', respectively.

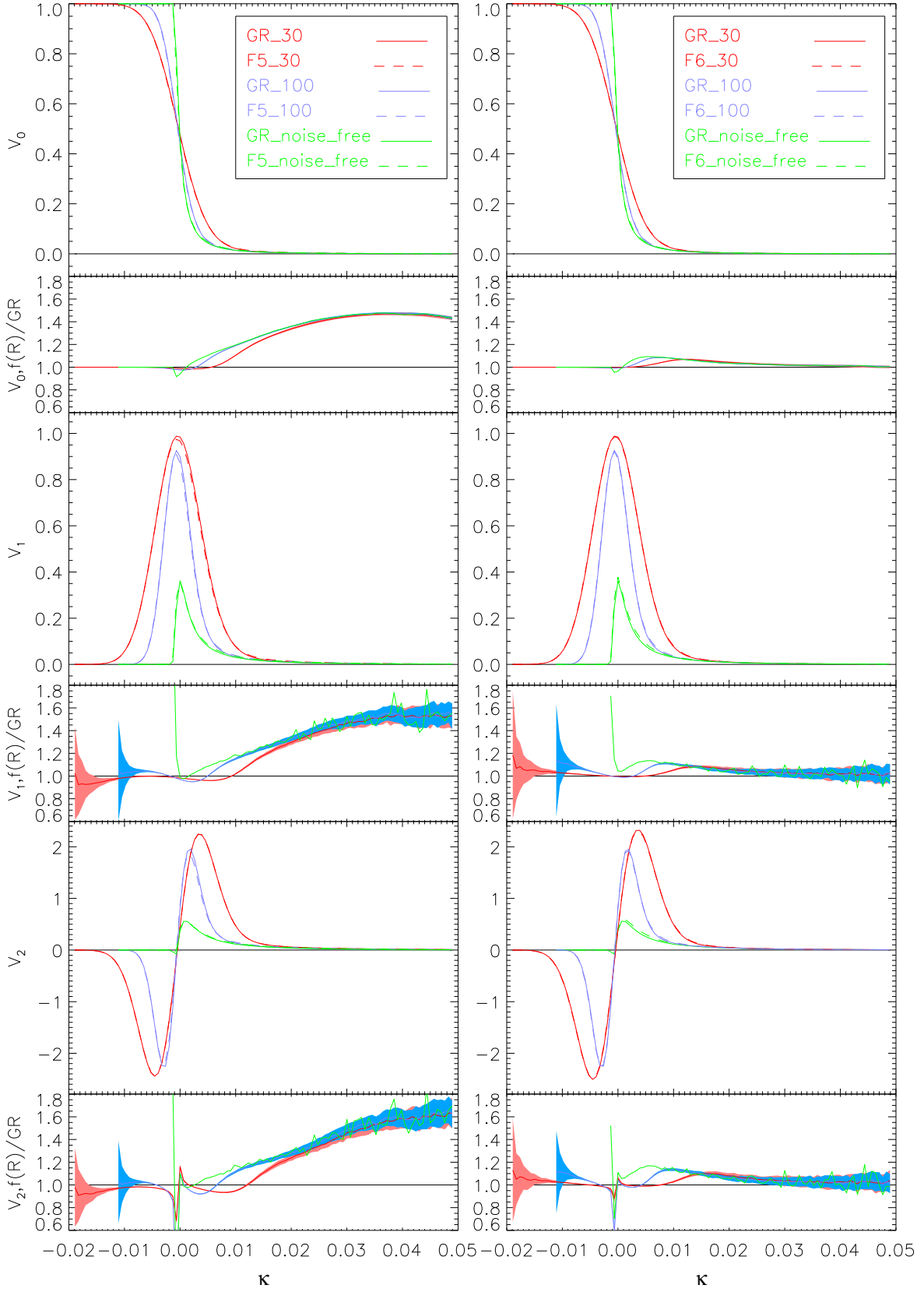


FIG. 3: Comparisons of the predicted MFs of lensing κ maps between the $f(R)$ and GR simulations for three different source number densities, $n_g = 30, 100$ and infinity (noise-free). In all cases the smoothing scale is taken to be $1'$. The left panel show comparison between F5 and GR models, while the right panel show comparison between F6 and GR models. The shaded regions show standard deviation of MFs from 100 mocked lensing maps.

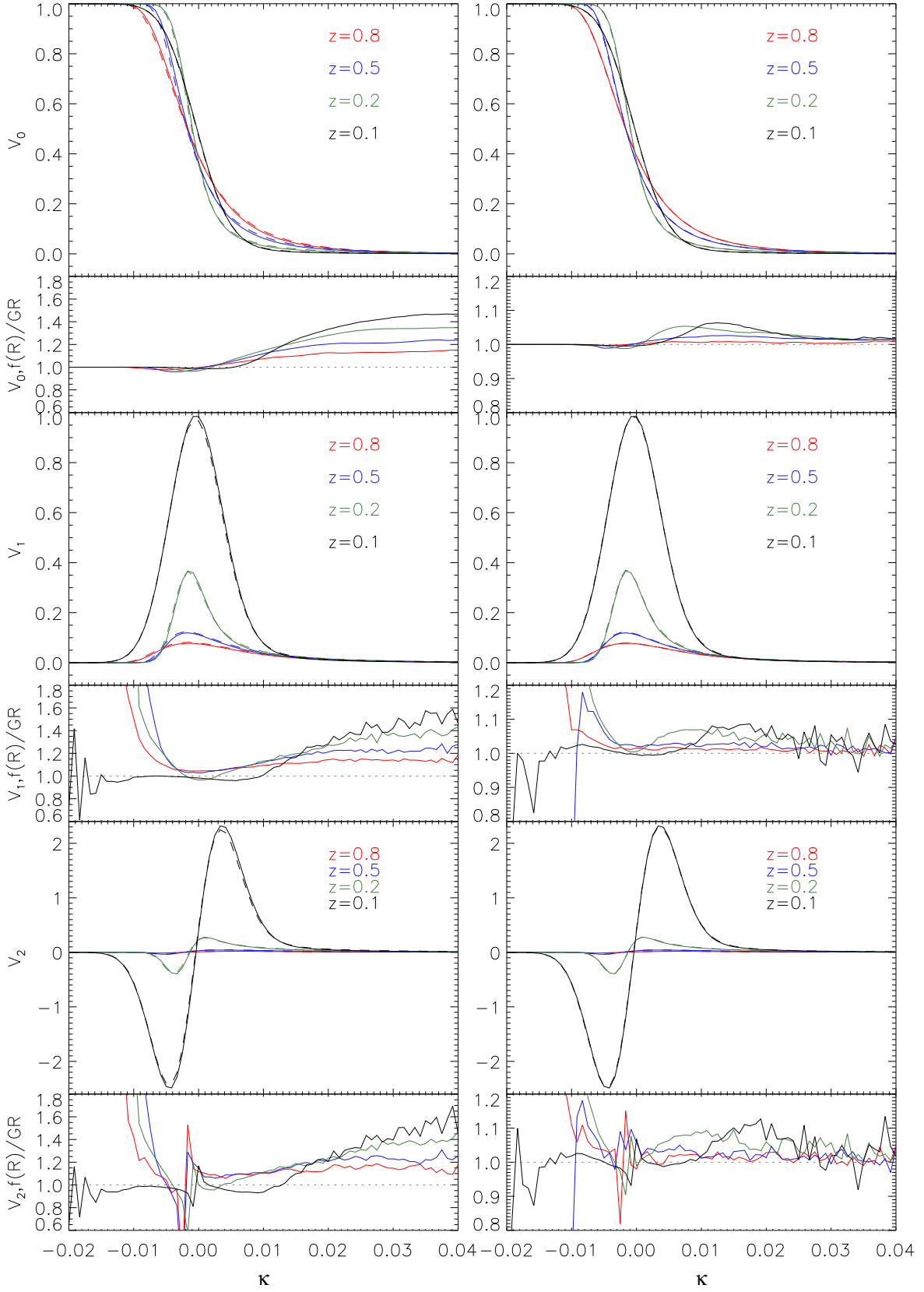


FIG. 4: Lensing MFs at $z = 0.8, 0.5, 0.2$ and 0.1 , with the same smoothing scale ($1'$) and source number density ($n_g = 30$). The left panels show the comparison between F5 and GR, while the right panels are the comparison between F6 and GR. The dashed (solid) lines are results for $f(R)$ gravity (GR).

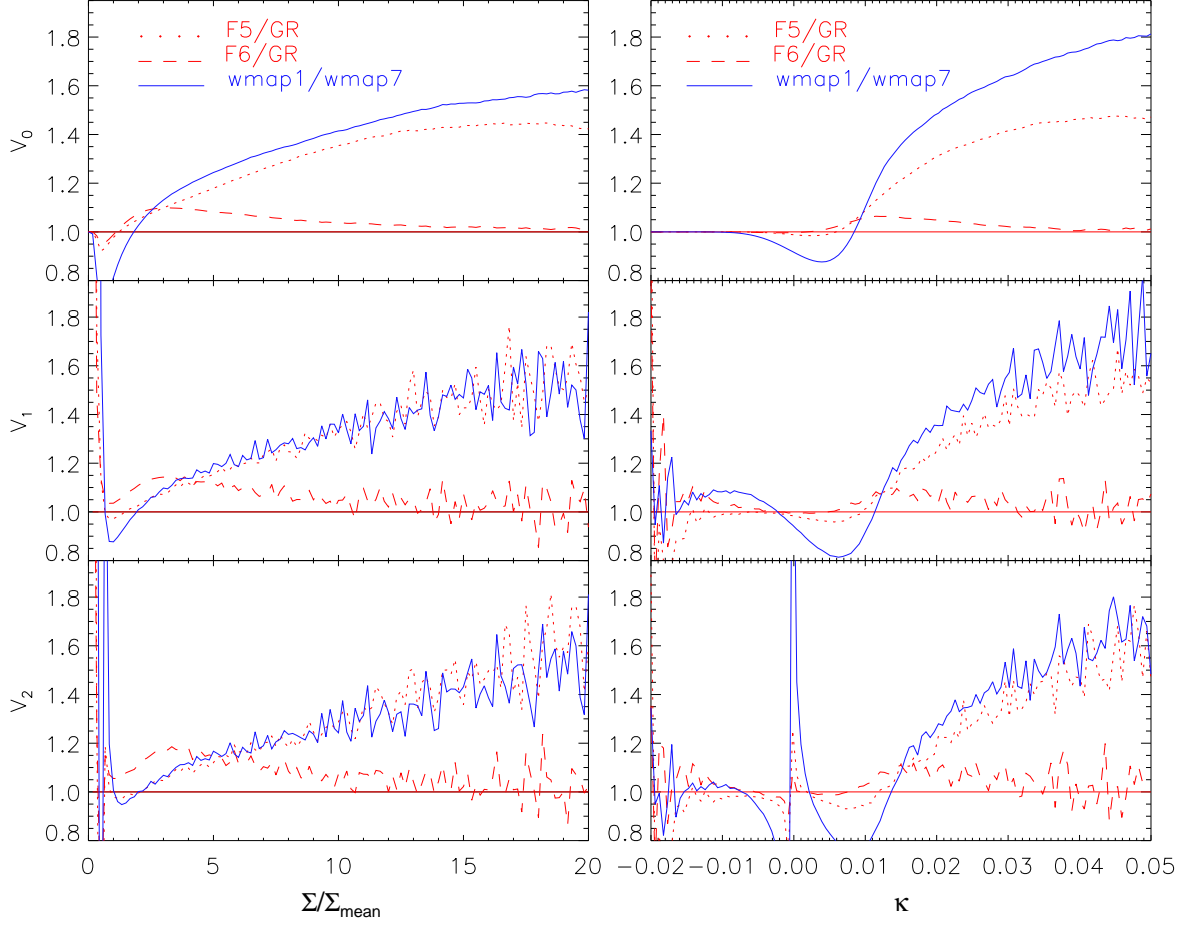


FIG. 5: Comparison of the effects on MFs from changing cosmological parameters from WMAP7 to WMAP1 and changing the gravity model (from GR to $f(R)$ gravity). The left panels show the results without noise, while the right panels assume a source number density $n_g = 30$. In all cases the smoothing scale is $1'$.